BBA - Biomembranes 1862 (2020) 183239

Contents lists available at ScienceDirect

BBA - Biomembranes

journal homepage: www.elsevier.com/locate/bbamem

The composition of phospholipid model bacterial membranes determines their endurance to secretory phospholipase A2 attack – The role of cardiolipin

Paulina Perczyk[a], Aneta Wójcik[a], Natalia Hachlica[a], Paweł Wydro[b], Marcin Broniatowski[a,*]

[a] Department of Environmental Chemistry, Faculty of Chemistry, Jagiellonian University, Gronostajowa 2, 30-387 Kraków, Poland
[b] Department of Physical Chemistry and Electrochemistry, Faculty of Chemistry, Jagiellonian University, Gronostajowa 2, 30-387 Kraków, Poland

ARTICLE INFO

Keywords:
Model bacterial membranes
Langmuir monolayers
Phospholipase A2
Grazing incidence x-ray diffraction
Brewster angle microscopy

ABSTRACT

Soil bacteria are decomposer organisms crucial for the biodegradation of organic pollutants, mineralization of dead organic matter and the turnover of biogenic elements. In their environment they are constantly exposed to membrane-lytic enzymes emitted to the soil by other microorganisms competing for the same niche. Therefore, the composition and structure of their membranes is of utmost importance for survival in the harsh environment. Although soil bacteria species can be Gram-negative or Gram-positive and their membranes differ significantly, they are formed by phospholipids belonging mainly to three classes: phosphatidylethanolamines (PE), phosphatidylglycerols (PG) and cardiolipins (CL). The correlation of the membrane phospholipid composition and its susceptibility to secretory membrane-lytic enzymes is widely unknown; thus, to shed light on these phenomena we applied the Langmuir monolayer technique to construct models of soil bacteria membranes differing in the mutual proportion of the main phospholipids. To characterize the systems we studied their elasticity, mesoscopic texture, 2D crystalline structure and discussed the thermodynamics of the interactions between their components. The model membranes were exposed to secretory phospholipase A2. It turned out that in spite of the structural similarities the model membranes differed significantly in their susceptibility to s-PLA2 attack. The membranes devoid of cardiolipin were completely degraded, whereas, these containing cardiolipin were much more resistant to the enzymatic hydrolysis. It also turned out that the sole presence of cardiolipin in the model membrane did not guarantee the membrane durability and that the interplay between cardiolipin and the zwitterionic phosphatidylethanolamine was here of crucial importance.

1. Introduction

Soil bacteria play an important role in the environment as the first-line decomposer organisms mineralizing the dead organic matter and degrading organic pollutants [1–3]. Many species, both Gram-negative as well as Gram-positive can also degrade persistent organic pollutants (POP), like polycyclic aromatic hydrocarbons and polychlorinated pesticides, which accumulate in the soils. POP can be easily mobilized by plant roots and included to the trophic chains endangering multiple plant and animal species; therefore, their elimination from the soils on the way of bioremediation is highly required [4–6]. There are some bacterial species for which POP can be the only carbon source [7,8], but for most of them POP are rather problematic nutrients as the native molecules and/or their metabolites can be highly toxic to multiple soil bacteria [9–11]. The first step of POP degradation is their inclusion into the bacterial membrane, which can occur directly, as POP are highly hydrophobic or indirectly by the inclusion of biosurfactant micelles solubilizing POP molecules [12,13]. The inclusion of POP into the membranes can lead to phase separations in the lipid matrix, lipid domain formation or generally the generation of multiple membrane defects [14,15]. The generation of membrane defects not only affects the membrane fluidity but can activate phospholipases from the A2 family – both those present in the bacterial cytoplasm as well as the secretory phospholipases (s-PLA2) present in the soil [16–19]. Bacteria prevent themselves against these phenomena trying to adjust the phospholipid composition to the environmental conditions [20–23]. It can be generalized that in the majority of Gram-negative and Gram-positive bacteria the membranes are composed of three phospholipid classes: phosphatidylethanolamines (PE), phosphatidylglycerols (PG) and cardiolipins (CL) [24,25]. They differ; however, between themselves in the mutual proportion of the phospholipids belonging to these three classes. In the inner membrane of *Escherichia coli* – the most

* Corresponding author.
E-mail address: broniato@chemia.uj.edu.pl (M. Broniatowski).

https://doi.org/10.1016/j.bbamem.2020.183239
Received 22 May 2019; Received in revised form 12 February 2020; Accepted 13 February 2020
Available online 28 February 2020

studied representative of Gram-negative bacteria PE dominate over the anionic phospholipids constituting 70–75% of the structural phospholipid pool [24–27]. On the other hand, in the Gram-positive bacteria the negatively charged phospholipids PG and CL dominate over PE [24,25]. Moreover, there are also known Gram-positive bacteria species completely devoid of PE, the membranes of which are formed solely by PG and CL [23,28,29]. Multiple studies performed on selected bacterial cell lines [30–32] liposomes [33,34] and Langmuir monolayers [35–39] underline the role of cardiolipin in the resistance of bacterial strains to antibiotics and membrane-lytic enzymes and their adaptations to harsh environmental conditions. However, the exact mechanisms correlating the composition of the bacterial membranes and their adaptations to particular environmental conditions are still not entirely understood.

To shed light on these phenomena we studied Langmuir monolayers formed of the PE, PG and CL phospholipids as versatile membrane models of Gram-negative and Gram-positive soil bacteria and correlated the composition of such model membranes with the membrane-lytic activity of secretory phospholipase A2. To follow the effect of the composition and mutual proportion of the phospholipids we prepared 9 different membrane models which can be divided onto three groups. The first were models mimicking Gram-negative bacteria inner membrane. In the models of this group all the mimetic membranes contained 70% of PE and the remaining 30% constituted anionic phospholipids PG and/or CL. The second and third group of models mimicked the Gram-positive membranes. In the second group the amount of PE was kept at the level of 20% as it is typical to multiple soil bacteria [24,25]; whereas the model membranes in the third group were formed solely of the anionic phospholipids PG and CL, as it happens in some soil bacteria [23,28,29]. It is a well-established tendency that in harsh environmental conditions bacteria switch the production of fatty acids from unsaturated or branched to saturated chains [21,40]; therefore, in our models we used saturated fatty acid lipids, all of them having the chains of myristic acid. Such a selection of phospholipids enabled the fruitful utilization of the experimental techniques as Grazing Incidence X-ray Diffraction (GIXD) and Brewster Angle Microscopy (BAM). The monolayers of unsaturated phospholipids are usually amorphous and cannot be characterized by GIXD. Moreover unsaturated phospholipids form usually homogeneous films, so their observation by BAM is also less convenient than in the case of saturated C14 and C16 phospholipids [41,42]. At the beginning of our studies we performed the thermodynamic characterization of the three possible binary systems CL/PE, PG/PE, CL/PG and a ternary system PE/PG/CL with the proportion of PE fixed at 20% in the full range of possible compositions. The model systems were characterized by BAM and the packing of the phospholipid molecules was characterized in the molecular scale by grazing incidence X-ray diffraction (GIXD). After the characterization of the physical, textural and crystalline properties of the mimetic membranes they were subjected to the action of phospholipase A2. In our studies we applied calcium dependent secretory PLA2 isolated from the venom of *naja naja mosambica* as a model of active secretory PLA2 emitted to the soil by different microorganisms. It turned out that the presence of cardiolipin in the membranes was crucial for their resistance against secretory PLA2; however, only its interplay with the zwitterionic phosphatidylethanolamine guaranteed the membrane durability.

2. Experimental

2.1. Materials

The 1,2-dimyristoyl-sn-glycero-3-phosphoethanolamine (DMPE), 1,2-dimyristoyl-sn-glycero-3-phospho-(1′-rac-glycerol) (sodium salt) (DMPG) and 1′,3′-bis[1,2-dimyristoyl-sn-glycero-3-phospho]-glycerol (sodium salt) (TMCL) were purchased from Avanti Polar Lipids as lyophilized powders of the purity 99%. The samples were sent with dry ice and were stored refrigerated at −20 °C. Spectroscopic grade chloroform (99.9%) stabilized by ethanol and spectroscopic grade methanol (99.9%) were purchased from Sigma-Aldrich. The lyophilized phospholipase A2 extracted from the venom of *naja naja mosambica* was also bought from Sigma-Aldrich as a lyophilized powder of the activity 1500 u/mg. PLA2 was kept refrigerated at −20 °C. Tris base (tris-hydroxymethylaminomethane) (99%), NaCl (99.5%), $CaCl_2$ (99.5%) and hydrochloric acid (36%, pure per analysis) were also provided by Sigma Aldrich. Ultrapure water of the resistivity 18.2 MΩ·cm was produced in our laboratory with the application of the Synergy Merck-MilliQ water purification system.

2.2. Solutions

The samples of the investigated phospholipids were weighted on the Mettler-Toledo analytical balance with the accuracy of 10 μg and dissolved in the chloroform/methanol 9/1 (v/v) mixture in class A glass volumetric flasks. Typically ca. 2.5 mg of the phospholipids were taken which gives the concentration of the stock solutions of ca. $3.5 \cdot 10^{-4}$ M for DMPE and DMPG and ca. $2.0 \cdot 10^{-4}$ M for TMCL. The stock solutions were kept refrigerated at −20 °C and mixed in the required proportion in amber glass vials just before experiments.

2.3. Subphase

In all experiments we applied the tris-saline buffer which is routinely used in the experiments with PLA2 [43–47]. The concentration of tris was 0.01 M, of NaCl 0.15 M and of $CaCl_2$ 0.005 M, so the ionic strength *I* of the solution was 0.165 M. The pH of the buffer was adjusted to 8.9 with the application of the proper volume of 1 M HCl solution. The lyophilized sample of PLA2 had the activity of 1500 u (One unit will hydrolyze 1.0 μmole of soybean L-α-phosphatidylcholine to L-α-lysophosphatidylcholine and a fatty acid per min at pH 8.9 and 25 °C). The PLA2 sample was dissolved in the above described tris-saline buffer, aliquots containing 20 u were moved to amber glass vials and frozen at −20 °C. In the experiments with PLA2 the appropriate volume of the concentrated enzyme solution (170 μl) was injected into the subphase (tris-saline) on the Langmuir trough to achieve finally the concentration of 0.01 u/cm^3 in the subphase.

2.4. Model membranes

As it was already mentioned in the introduction, 9 model membranes were prepared. The compositions of the models are summarized in Table 1.

2.5. Techniques

2.5.1. Langmuir technique

Three different Langmuir troughs were used in the experiments. For the registration of the π-A isotherms applied for the further thermodynamic considerations and performing the experiments with the

Table 1
Composition of the membrane models. The mole ratio X_i of an i^{th} component is defined as follows: $X_i = \frac{N_i}{\sum_1^i N_i}$, where N_i is the number of the molecules of the i^{th} component.

Model	X(DMPE)	X(DMPG)	X(TMCL)
GNC	0.7	–	0.3
GNCG	0.7	0.15	0.15
GNG	0.7	0.3	–
GPC	0.2	–	0.8
GPCG	0.2	0.4	0.4
GPG	0.2	0.8	–
BAC	–	0.25	0.75
BACG	–	0.5	0.5
BAG	–	0.75	0.25

enzyme a KSV-NIMA middle (KN 2002) double-barrier trough of the area of 275 cm^2 was applied. The trough was equipped with: a centrally located rectangular deposition well, an injection port and a magnetic stirrer which enabled the performance of penetration tests. BAM experiments were performed on the double barrier KSV-NIMA 1006 trough (nominal area of 841 cm^2). In the Sirius beamline of the Soleil synchrotron a single barrier Riegler&Kirstein (R&K) trough of the area of ca. 500 cm^2 was installed. All the troughs were manufactured from a single block of Teflon without any glued elements. After each experiment the monolayer material and the subphase was removed from the troughs with a vacuum aspirator and the Teflon elements were cleaned with a tissue soaked in chloroform, followed by isopropanol and rinsed with plentiful of MilliQ water. All the experiments were performed on the tris-saline buffer. In a typical experiment the required volume of the chloroform/methanol solution of the phospholipids was spread on the surface of the subphase on Langmuir trough by Hamilton analytical syringes. 10 min were left for the spreading solvent evaporation after which the monolayers were compressed with the compression rate of 20 $cm^2 \cdot min^{-1} \cdot mol.^{-1}$. All the experiments were performed at 20 °C and the temperature of the subphase was kept constant (± 0.1 °C) by Julabo water circulating bath. The surface pressure was monitored with the Wilhelmy-type electrobalance with a plate of filtration paper (Whatman, ashless) as the surface pressure sensor. The accuracy of the sensor was ± 0.05 mN/m. All the π-A isotherms were measured at least three times and the uncertainty of the mean molecular area A was ca. 1 $Å^2$/molecule.

Compression modulus, C_S^{-1} was calculated from the π-A isotherms according to its definition [48]:

$$C_S^{-1} = -A\left(\frac{\partial \pi}{\partial A}\right)_{T,p,n}$$

where the indices T, p and n indicate the constant temperature, pressure and composition of the monolayer, respectively.

The excess Gibs energy of mixing ΔG^{exc} was calculated according to its definition [49]:

$$\Delta G^{exc} = N_A \int_0^{\pi} A^{exc} d\pi$$

N_A – Avogadro number, A^{exc} – excess mean molecular area:

$$A^{exc} = A_{1-n} - A_{id}$$

$A_{1\text{-}n}$ – area observed for a given π for an n-component monolayer

$$A_{id} = \sum_1^n A_n X_n$$

X_n – mole ratio of the n^{th} component of the monolayer, A_n – mean molecular area observed at a given π value for the one-component monolayer of the n^{th} component.

2.5.2. Experiments with the enzyme

In a standard experiment the Langmuir monolayer was compressed to 20 mN/m, after which the surface pressure was kept constant. 20 min were left for monolayer stabilization after which the concentrated solution of PLA2 (170 μl) was injected via the injection port deep into the well of the Langmuir trough. The subphase in the well was stirred with a magnetic stirrer to facilitate the uniform diffusion of the enzyme below the monolayer. In this kind of experiments the mean molecular area vs time (A-t) curves were registered. $t = 0$ was acquired as the moment of PLA2 injection. The A-t curve was monitored at least 1 h or longer if necessary. All the experiments were repeated at least two times.

2.5.3. Brewster angle microscopy (BAM)

In these studies UltraBAM instrument (Accurion GmbH, Goettingen, Germany) equipped with a 50 mW laser emitting p-polarized light at a wavelength of 658 nm, a 10× magnification objective, polarizer, analyzer and a CCD camera was used. The spatial resolution of the microscope was 2 μm. The foregoing apparatus and the Langmuir trough were placed on the table (Standa Ltd., Vilnius, Lithuania) equipped with active vibration isolation system (antivibration system VarioBasic 40, Halcyonics, Göttingen, Germany).

2.5.4. Grazing incidence X-ray diffraction (GIXD)

The experiments were performed on the SIRIUS beamline at SOLEIL synchrotron (Gif-sur-Yvette, France) using the dedicated liquid surface diffractometer. The Langmuir trough (R&K Gmbh electronics, Germany) was mounted on the goniometer in a gas tight box with Kapton windows. Before each experiment, the canister was sealed and flushed with helium to reduce the oxygen level. After at least 30 min, the monolayer was compressed to the target surface pressure of 25 mN/m. Surface pressure was kept constant at this value during the entire experiment by the Langmuir trough operating software, which counterbalance the monolayer relaxation by changing the mean molecular area (compressing or expanding slowly the monolayer if necessary to keep the surface pressure constant). The length of the X-ray beam was 1.565 Å. The detailed construction of the diffractometer working at the SIRIUS beamline and the parameters of the synchrotron beam applied in the GIXD experiments are described on the SOLEIL web site (www.synchrotron-soleil.fr). The scattered signal was detected using Pilatus3 detector (Dectris Ltd., Switzerland). This detector is used as 1D detector through the combined use of a Soller slits collimator oriented vertically to fix the in-plane 2θ resolution and an integration of the 2D image horizontally to obtain a 1D spectrum. The achieved resolution was about 0.002 $Å^{-1}$. The spectra were obtained by scanning the in-plane 2θ angle. At each point, the vertically scattered intensity was recorded to obtain finally the intensity map $I(Q_{xy},Q_z)$ where Q_{xy} is the scattering vector component in the monolayer plane, and Q_z is the vertical component along the z-axis. The $I(Q_{xy},Q_z)$ diffractograms were integrated along the vertical distribution of Q_z to obtain the Bragg peaks $I(Q_{xy})$. Simultaneously the spectra were integrated over the Q_{xy} values to obtain the Bragg rods, $I(Q_z)$. The estimation of the full width at half maximum (FWHM) of Bragg peak enables the calculation of the L_{xy} parameter, which is related to the range of 2D crystallinity, whereas from the FWHM of Bragg rod the L_z parameter related to the length of the scattering moiety can be gained. These parameters are calculated according to the Scherrer formula: $L_{xy} \approx 0.88 \cdot 2\pi/FWHM_{peak}$, $L_z \approx 0.88 \cdot 2\pi/FWHM_{rod}$.

3. Results and discussion

3.1. Thermodynamic considerations for the investigated binary and ternary phospholipid systems

At the beginning of the experiments the binary monolayers of the three essential phospholipids were investigated: TMCL/DMPE, DMPG/DMPE and TMCL/DMPG. The resulting π-A isotherms are presented in SFig1–SFig3 of the Supporting materials. After the binary systems a ternary system containing all the three investigated phospholipids was investigated. This system was studied in search of the convenient Gram positive bacteria membrane models containing DMPE. X(DMPE) in the system was fixed at X(DMPE) = 0.2 and X(DMPG) was changed with the step of 0.1. The resultant π-A isotherms for the ternary system are presented in SFig4 in the Supporting materials. The sets of π-A isotherms enabled the calculations of the excess Gibbs energy of mixing and the ΔG^{exc} – X plots are presented in Fig. 1.

Generally the sign of ΔG^{exc} is interpreted as follows: negative sign indicates that the interaction between different molecules (e.g. TMCL and DMPE) are more attractive than in the one component monolayer between same molecules. Vice versa the positive sign denotes the less attractive or repulsive character of the interactions [49]. In the system TMCL/DMPE the sign of ΔG^{exc} is positive at low X(DMPE) of 0.1 and 0.2, and negative for X(DMPE) = 0.7 and 0.9; whereas for X

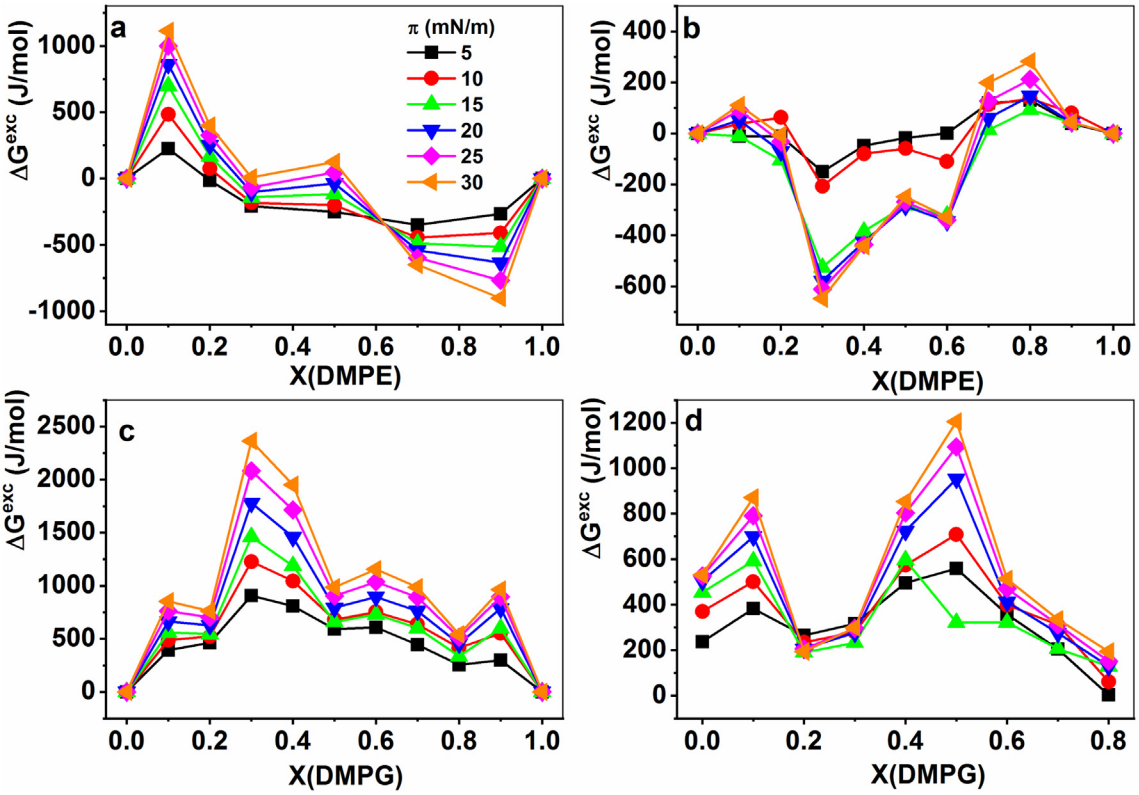

Fig. 1. ΔG^{exc} – X(phospholipid) plots for the investigated systems: a) TMCL/DMPE; b) DMPG/DMPE; c) TMCL/DMPG and d) DMPE/TMCL/DMPG at X(DMPE) = 0.2.

(DMPE) = 0.3 and 0.5 ΔG^{exc} is close to 0. Two mole fraction in this system correspond to the model membranes investigated in our studies: GPC, for which X(DMPE) = 0.2 and GNC for which X(DMPE) = 0.7. For both the ratios the absolute values of ΔG^{exc} range from 0 to ca. 500 J/mol. depending of the compression degree of the monolayer (surface pressure); thus, the values of ΔG^{exc} are relatively small. The sign of ΔG^{exc} for GPC is positive and for GNC negative. Thus, at the first approximation it is probable that the phospholipid molecules in the GNC model membrane are somehow better organized than in the GPC monolayer; however, this hypothesis should be verified by the other applied experimental techniques. In the system DMPG/DMPE ΔG^{exc} is close to 0 for X(DMPE) ranging from 0 to 0.2 and from 0.7 to 1, whereas for the mole ratios of DMPE ranging from 0.3 to 0.6 it is negative. On the basis of the course of the ΔG^{exc} – X(DMPE) curve it can be inferred that the two-chained phospholipid molecules mix practically ideally with eventual small negative deviation from ideality. Within this system we have two model membranes: GPG at X(DMPE) = 0.2 and GNG at X(DMPE) = 0.7. For both models ideal miscibility of the components can be expected. In the system TMCL/DMPG the sign of ΔG^{exc} is positive and ΔG^{exc} achieves quite high values of ca 2000 J/mol for X(DMPG) = 0.3 and 0.4. The observed trend proves that although TMCL is structurally closely related to DMPG their interactions in a binary film are energetically unfavorable. This is in accordance with the measurements performed for similar systems by other authors. Crossnigg and co-authors [50] formed liposomes from TMCL and DPPG testing a wide range of mutual mole ratios. Their DSC and wide and small angle (WAXD and SAXD) X-ray diffraction experiments proved that the miscibility of TMCL with DPPG was far from ideality and that for some compositions phase separation of both components was highly probable. The less attractive interactions between TMCL and DMPG molecules in the binary system can be connected with the charge of the polar headgroup. Within the TMCL/DMPG system we have three model membranes: BAC at X(DMPG) = 0.25, BACG at X(DMPG) = 0.5 and BAG at X(DMPG) = 0.75. The highest values of ΔG^{exc} can be noticed for BAC and what should be underlined there are significant differences between the ΔG^{exc} levels depending on the surface pressure value as for π = 5 mN/m the value of ΔG^{exc} was ca. 700 J/mol and for π = 30 mN/m it was ca. 2500 J/mol, so it is possible that lateral phase separation can occur upon the BAC film compression. For BACG and BAG the values of ΔG^{esc} are comparable ranging from ca. 500 J/mol at π = 5 mN/m to ca. 1000 J/mol for π = 30 mN/m. Finally in the ternary system DMPE/TMCL/DMPG at X(DMPE) fixed at 0.2 ΔG^{exc} is positive for all the proportions but the values of ΔG^{exc} are rather low for most of the compositions. Two maxima can be observed in the plot for the compositions DMPE/TMCL/DMPG 0.2/0.7/0.1 and 0.2/0.3/0.5. Within this system one of the investigated model membranes can be identified. It is GPCG at X(TMCL) = X(DMPG) = 0.4. For GPCG ΔG^{exc} ranges from ca. 400 J/mol at π = 5 mN/m to 800 J/mol at π = 30 mN/m. For the last system GNCG for which X(DMPE) = 0.7, X(TMCL) = X(DMPG) = 0.15 the value of ΔG^{exc} can be predicted being close to 0 on the basis of the ΔG^{exc} -X plots presented in panels a and b of Fig. 1.

3.2. Characterization of the model membranes

In the next step of the investigation larger volumes of the mixed binary and ternary solutions corresponding to the 9 model membrane-mimicking monolayers were prepared in 5 cm^3 volumetric flasks. π-A isotherms were registered upon the compression of the model membranes and compression modulus values were calculated and plotted in the form of C_S^{-1} – π dependences. All these curves are presented in Fig. 2.

For the Gram-negative models characteristic plateau can be observed in the course of the π-A isotherms which is the manifestation of the LE-LC phase transition. Such a plateau is present also in the π-A isotherms registered for the one-component monolayers of the investigated lipids [51,52]. The average surface pressure corresponding to the plateau is comparable with these observed for one component monolayers [51]. At further compression a very steep region in the

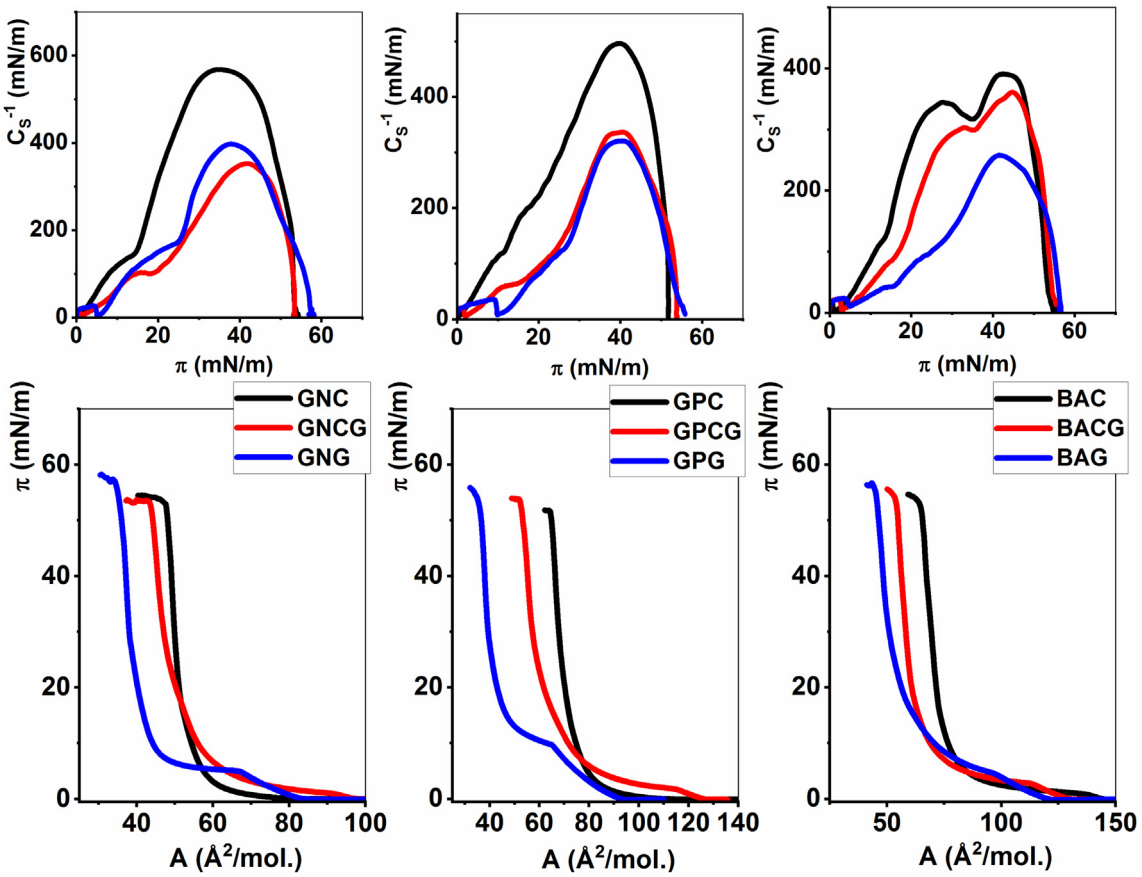

Fig. 2. π-A isotherms and C_S^{-1} – π dependences for the investigated model bacterial membranes.

isotherms can be observed corresponding with the low elasticity of the films. Indeed, the C_S^{-1} values indicate that the monolayers achieve the ordering typical to the solid (S) state of the monolayer [48]. The Gram-positive bacteria membrane models from the GP series differ more significantly between each other than it was observed for the GN models, which is understandable, as their compositions changes more significantly from model to model. GPC – the monolayer rich in cardiolipin has a solid character achieving the limiting C_S^{-1} value of 250 mN/m at the surface pressure of ca. 25 mN/m. The two other models GPCG and GPG remain mainly in the LC state with a narrow window of surface pressures for which C_S^{-1} exceeds 250 mN/m indicating the 2D solid state ordering. In the series of the BA models of Gram-positive bacteria membranes the isotherms have similar course but they move successively toward lower mean molecular areas as the ratio of cardiolipin decreases. BAC and BACG monolayers behave similarly upon the compression. These monolayers are stiff and poorly compressible remaining in the solid state for a wide range of surface pressures. In contrast, the BAG monolayer is much more elastic which results in considerably lower C_S^{-1} values, as the BAG monolayer remains in the LC state till the end of the monolayer compression.

The monolayers mimicking the bacterial membranes were visualized upon their compression with the application of Brewster angle microscopy and the resultant BAM images collected for the GN models are presented in Fig. 3.

Regarding their mesoscopic textures the monolayers from the GN series behave similarly. Large dendritic condensed domains of the diameter of ca. 40–50 μm form in the monolayer at the surface pressure ranging from 5 to 10 mN/m, so at 10 mN/m the domains are well developed. In the case of GNG the domains are less numerous and smaller with the average diameter of 30 μm. The domains at 10 mN/m are separated with multiple darker regions of the monolayers, which at 10 mN/m remain in the equilibrium between the LE and LC states. The further compression of the monolayers to 20 mN/m leads to partial merge of the condensed domains, which is much progressed in the case of GNCG. On the other hand, the domains in the GNG monolayer remain still separated from each other which is in accordance with the lower C_S^{-1} values observed for this monolayer at this surface pressure value and the higher transition value (see Fig. 2). The further compression to 30 mN/m leads to the fusion of the LC domains and the formation of practically homogenous monolayers which according to the C_S^{-1} – π curves are in the S state. The presence of numerous 3D aggregates should be underlined at these conditions. Their presence indicates that the models in the GN series are quite unstable and that some lipid molecules tend to phase separate forming an additional 3D phase. The diameter of the 3D domains is very small and for many of the aggregates it falls below 2 μm, that is the resolution limit of the microscope. It results in the interference effects like concentric circles or Moire patterns visible in the photos.

As it can be noticed in Fig. 4 the models from the GP and BA series differ significantly regarding their mesoscopic texture. The domains evolving upon the compression of the monolayers from the GP series are very similar to those described for the GN series. Large dendritic domains with their diameters of ca. 50 μm evolve between 5 and 10 mN/m (10–15 mN/m for GPG). At 20 mN/m the domains remain separated from each other which differentiate them from the analogous models in the GN series. At 30 mN/m the merging of the domains is highly advanced, but the monolayers are not entirely homogeneous. The main difference between the GN and GP series regards the presence of 3D aggregates at the air/water interface. In the case of the models of the GN series the aggregates are numerous already at 20 mN/m, whereas in the case of the monolayers from the GP series some tiny aggregates can be observed for GPG and GPCG model membranes at 30

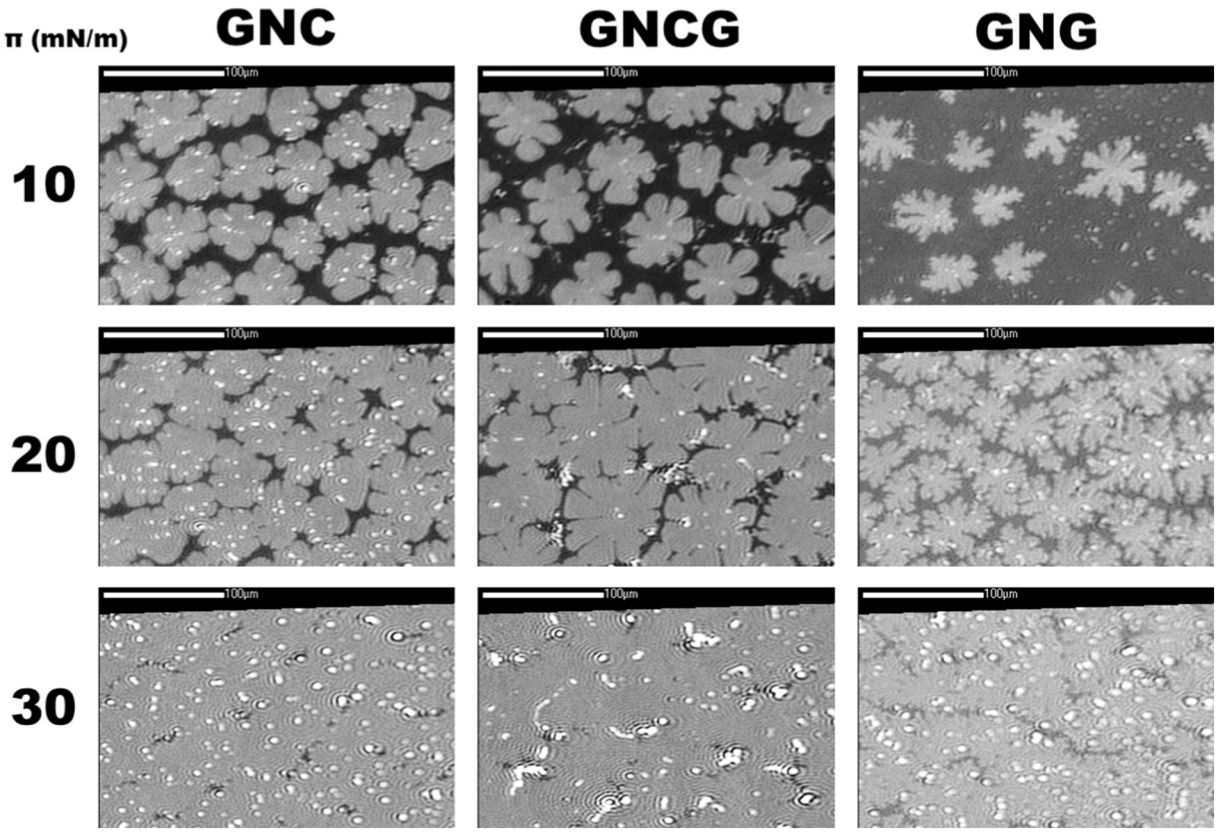

Fig. 3. Representative BAM images for the models of Gram negative bacteria membranes. The scale bar denotes 100 μm.

mN/m, whereas no aggregates can be noticed in other BAM images. The lack of aggregates in the GP series and their presence in GN series can be strictly related to the net charge of the headgroups of the phospholipids in the model membranes. In the GP series the anionic phospholipids dominate and the repulsion between the headgroups can effectively limit the tendency to aggregate. The model membranes from the BA series differ considerably from the GN and GP series. The domains are small and circular. The average diameters at 10 mN/m are ca. 12 μm for BAC, 20 μm for BACG and only 5 μm for BAG. The rise of the surface pressure leads to the fusion of the domains which do not considerably increase their dimension. The merging process is less advanced in the BACG monolayer, whereas in the BAG model membrane the domains remain completely separated increasing their average diameter to ca. 15 μm. At 30 mN/m the BAC monolayers are practically homogenous whereas in the BACG and BAG monolayers some boundaries between the domains can still be observed. No 3D aggregates form in the monolayers from the BA series within the observation range of surface pressures. It should be underlined that the size of a typical bacterium is ca. 2 μm; thus, they are smaller than the diameters of the domains visualized in Figs. 3 and 4. Discussing BAM images one should always underline that this is the so-called mesoscopic scale [42]; however, the observed morphologies of the domains and their evolution with the surface pressure rise reflect often the trends regarding submicroscopic condensed domains which are the building blocks of the mesoscopic structures. For example it can be inferred from the drastically different textures of the monolayers belonging to the GP and BA

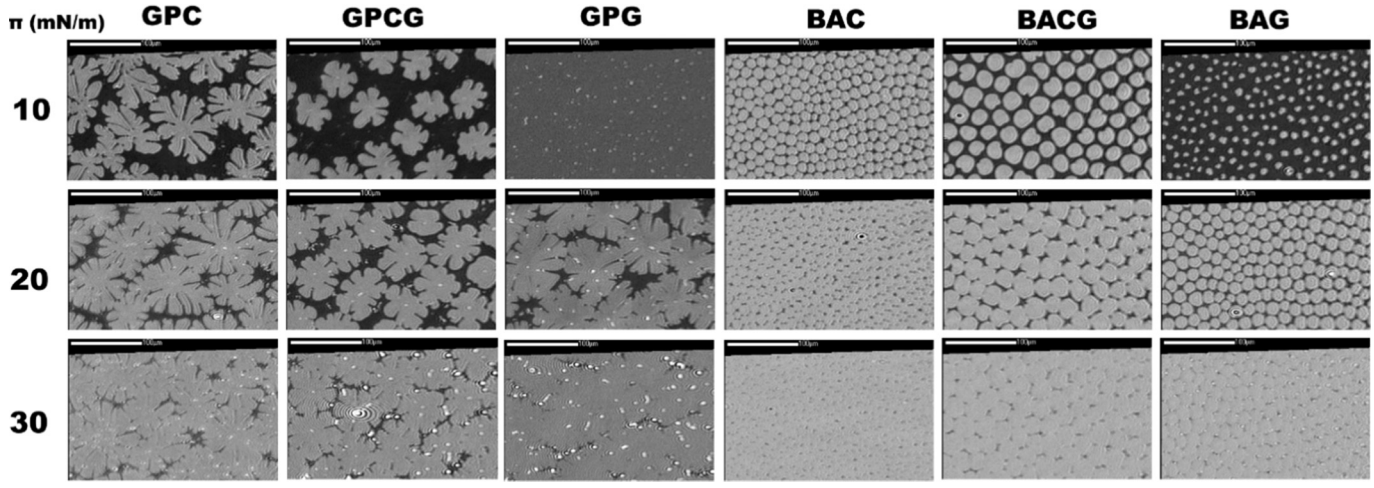

Fig. 4. Representative BAM images for the models of Gram positive bacteria membranes. The scale bar denotes 100 μm.

series that also in the real Gram-positive bacteria significant differences in the membrane organization can be expected between the membranes containing the phospholipids from the PE class and these formed entirely from anionic phospholipids.

As it was underlined BAM images provide the insight into the mesoscopic structure of the model membranes and the conclusions correlating the monolayer texture and molecular organization within the domains have always the indirect character. Thus, to obtain the access to the molecular scale and to discuss the differences between the model membranes with Ångstrom resolution we applied the Grazing Incidence X-ray diffraction technique. GIXD provides direct information about the molecular packing in the monolayer, provided that the monolayer domains are 2D crystalline. All the 9 model membranes were included into the GIXD experiments. Their components TMCL, DMPG and DMPE form 2D crystalline domains which was reported previously in multiple publications [15,52–54]. However, the mixing of two kinds of phospholipid molecules can lead to the amorphization of the condensed domains, so the first step of our GIXD experiments was the check if for the model membranes any diffraction signal can be observed. It turned out that for all the 9 monolayers a strong diffraction signal was observed in the GIXD experiment. For most of the monolayers only one signal with its intensity maximum at $Q_z = 0$ Å^{-1} was observed, meaning the hexagonal unit cell and the upright orientation of the hydrophobic chains at the air/water interfaces. The results for four of the investigated monolayers: two Gram negative (GNC and GNG) and two Gram positive (BAG and GPG) are presented in Fig. 5. The results for the other model membranes and the one-component monolayers of the investigated phospholipids are accessible in the Supporting materials (SFig5–SFig10). The lattice parameters (a, b, γ), the area of the unit cell A, and the L_{xy} parameter denoting the range of 2D crystallinity are gathered in Table 2.

Table 2
Essential parameters extracted from the GIXD data.
The uncertainty of Q_{xy} is ± 0.002 Å^{-1}, so the uncertainty of the lattice parameters a and b is ca. 0.01 Å.

System	Q_{xy}, Q_z (Å^{-1}, Å^{-1})	(a, b, γ) (Å, Å, deg)	A (Å^2)	L_{xy} (Å)	τ (deg)
DMPE	1.466, 0	a = b = 4.95, 120	21.2	430 (± 7)	0
DMPG	1.468, 0	a = b = 4.94, 120	21.1	446 (± 10)	0
TMCL	1.474, 0	a = b = 4.92, 120	21.0	635 (± 5)	0
GNC	1.462, 0	a = b = 4.96, 120	21.3	718 (± 5)	0
GNCG	1.459	a = b = 4.97, 120	21.4	523 (± 12)	0
GNG	1.452, 0	a = b = 5.00, 120	21.6	354 (± 5)	0
GPC	1.462, 0	a = b = 4.96, 120	21.3	727 (± 6)	0
GPCG	1.458, 0	a = b = 4.98, 120	21.4	572 (± 8)	0
GPG	⟨−1,1⟩ 1.439, 0.264 ⟨0,2⟩ 1.453, 0	5.06, 8.65, 90	43.7 (21.9 per chain)	$L_{\langle -1,1\rangle}$ = 263 (± 7) $L_{\langle 0,2\rangle}$ = 369 (± 6)	12.0 (± 0.1)
BAC	1.462, 0	a = b = 4.96, 120	21.3	718 (± 5)	0
BACG	1.460, 0	a = b = 4.97, 120	21.4	660 (± 5)	0
BAG	⟨−1,1⟩ 1.450, 0.110 ⟨0,2⟩ 1.460, 0	5.02, 8.61, 90	43.2 (21.6 per chain)	$L_{\langle -1,1\rangle}$ = 213 (± 5) $L_{\langle 0,2\rangle}$ = 783 (± 5)	5.0 (± 0.2)

For the model membranes of Gram negative bacteria (GN series) compressed to 25 mN/m one intense diffraction signal is present in the I (Q_{xy}, Q_z) intensity map. The maximum of the intensity of the diffraction

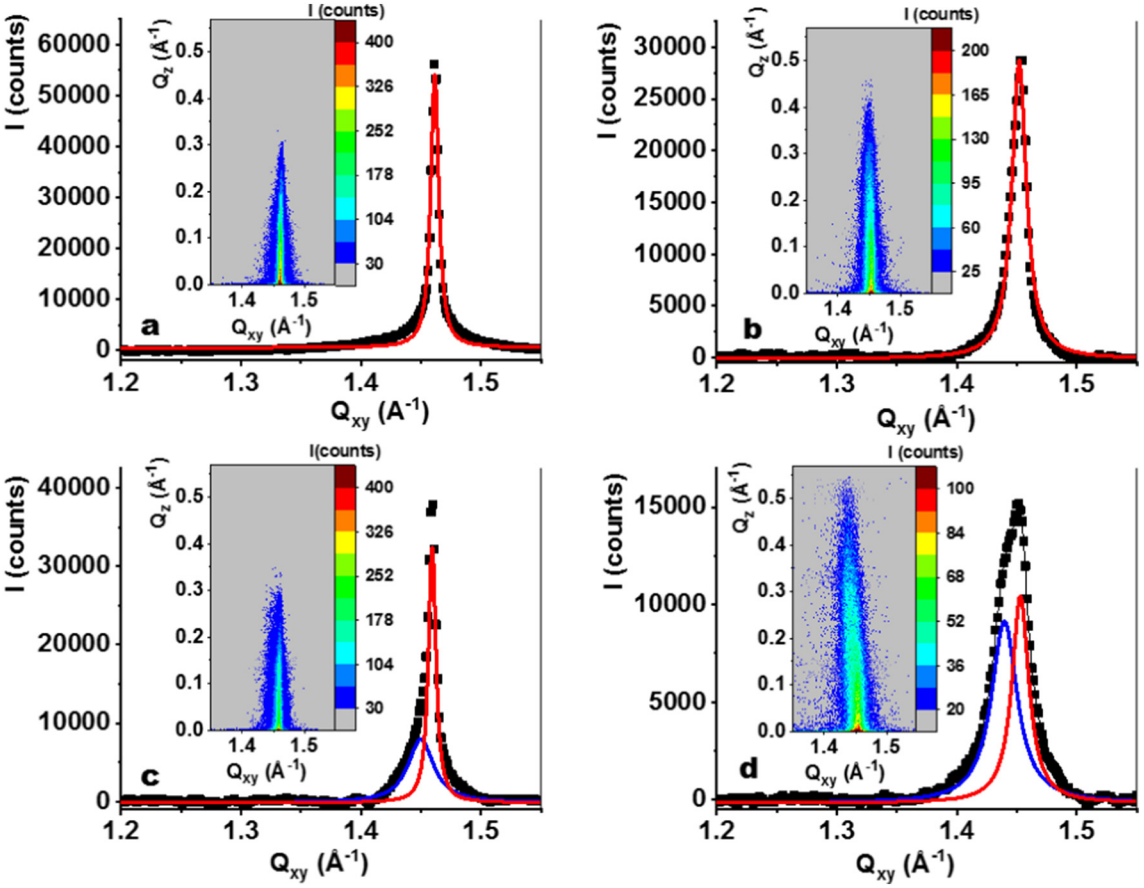

Fig. 5. GIXD data: Bragg peaks and intensity maps ($I(Q_{xy},Q_z)$) for the selected membrane-mimicking monolayers: a) GNC, b) GNG, c) BAG, d) GPG. The solid lines in the Bragg peak plots are Lorentz fits to the experimental data.

signal is observed at $Q_z = 0$, which means that the hydrocarbon chains of the phospholipid molecules forming the 2D crystalline nanodomains are oriented upright at the air/water interface and that the 2D unit cell is hexagonal [55]. The length of the edge *a* of the unit cell is comparable for all three models from the GN series and the one component monolayers of the investigated phospholipids. The L_{xy} parameter denoting the range of crystallinity has the greatest value of 718 Å for GNC. This value is noticeably greater than for the one-component phospholipid films, meaning that the energetically beneficial interactions of DMPE and TMCL lead to the increase of the 2D crystallinity within the model membrane. The L_{xy} parameter decreases successively via 523 Å observed for GNCG to 354 Å observed for GNG. This trend underlines the role of cardiolipin as the promotor of the model membrane long-range ordering. Similar trend regarding the L_{xy} parameter was also observed for the GP series of the model bacterial membranes. In the GP series the model membranes GPC and GPCG, that is these containing cardiolipin were crystalline with the scattering moieties (myristic acid chains) oriented upright. Generally, the organization of the molecules and the range of crystallinity were very similar as in the GN series. It is interesting, as the ΔG^{exc} values were negative for the GN models and positive for the GP models, so we expected that the differences originate from the molecular packing. However, it should be underlined that the scatterers in the GIXD method are the acyl chains, whereas the polar headgroups are usually not oriented periodically. On the other hand, the interactions between the headgroups provide the most important increments to the energy of the intermolecular interactions which is finally reflected in the sign and value of ΔG^{exc}.

For two of the models emulating the Gram positive bacteria, these containing large amount of DMPG, i.e. BAG and GPG two diffraction signals can be discerned in the $I(Q_{xy}, Q_z)$ contour map. One of them indexed ⟨0,2⟩ has its intensity maximum at $Q_z = 0$, whereas the other indexed as ⟨−1,1⟩ has the intensity maximum over the horizon at $Q_z > 0$. The area of the ⟨−1,1⟩ signal is approximately two times bigger than of the ⟨0,2⟩, which is typical to the centered rectangular 2D crystal lattice [55]. The deformation of the hexagonal lattice typical to the other models of the bacterial membranes investigated in our studies originates from the tilt of the hydrocarbon chains of the phospholipid molecules from the monolayer normal. The tilt angle in the BAG model membrane is very small, at the level of 5.0 °, whereas in the GPG model membrane the tilt is much noticeable being 12.0°. The range of 2D crystallinity measured by the L_{xy} parameter is very high in the BA series, with L_{xy} exceeding 700 Å.

3.3. Model membrane composition and the activity of PLA2

In our project we subjected all the 9 studied here models to the action of s-PLA2. As the model of s-PLA2 present in the soil we applied the Ca^{2+}-dependent s-PLA2 isolated from the venom of the spitting cobra *naja naja mosambica* as it is characterized by high activity (1500 u/mg) and wide substrate specificity. It was proved in the literature that the structure of the phospholipid binding active site of prokaryotic s-PLA2 has a similar aminoacid sequence, folding and ternary structure as the active site of eukaryotic s-PLA2s [17,56,57]; thus the highly active venom s-PLA2 can be treated as a versatile model of the prokaryotic PLA2s secreted to the soil. The model membranes were spread on the tris-saline buffer, compressed to 20 mN/m, left at constant surface pressure to stabilize for 20 min, after which the concentrated solution (170 μl) of s-PLA2 was injected into the well of the Langmuir trough. The evolution of surface area in time (A-t curve) was monitored after the enzyme injection. Similar experiments were performed for the one-component phospholipid monolayers formed by DMPE, DMPG or TMCL and the resultant A-t curves are shown in the Supporting materials in SFig11. Here in Fig. 6 we present the A-t curves registered for the model bacterial membranes after the s-PLA2 injection.

In a typical A-t curve registered after the injection of a Ca^{2+} dependent s-PLA2 to the buffered subphase below a model phospholipid membrane two distinct regions can be discerned. In the first region starting in the moment of the enzyme injection the change of A with time is relatively small; whereas in the second region the value of dA/dt (the slope of the curve) increases considerably. The two parts of the experiment are called the lag and the burst phases, respectively [58]. If two tangent lines are fitted to both regions of the A-t curve their intersection defines the so-called lag time, t_L. Such a characteristics of the A-t curve, the existence of t_L and the low rate of the enzymatic reaction in the first period is connected with the diffusion of s-PLA2 from the subphase to the air/water interface, the docking of the enzyme at the borders of the LC phospholipid domains and the appearance of first lysolipid molecules [58–61]. Many authors claim that the presence of lysolipid molecules activates the enzyme and leads to the second period of the experiment, called the burst phase, manifested in the steep region of the A-t curve [45,58]. It is highly probable that the lysolipid molecules do not activate the enzyme directly by binding to it, but their appearance initiates phase separation processes and the generation of new membrane defects, which considerably facilitates the docking of s-PLA2 to the model membrane [45,62–64]. It can be noticed from Fig. 6 that the enzyme was inactive toward one of the model membrane, GPC. In the other 8 experimental systems two regions can be discerned in the A-t curves in agreement with the above discussion. Regarding the course of the A-t dependences the curves can be divided onto two groups: for some of the systems (GNC, GNCG, GNG, GPG) the temporal fall of the mean molecular area in the burst phase is linear; whereas for the other (GPCG, BAC, BACG and BAG) it is rather sigmoidal. This behavior can be correlated with presence of cardiolipin in the model membrane at high molecular ratio. Indeed, the A-t curve for the one-component TMCL monolayer after the s-PLA2 injection is a sigmoid (see SFig11 in the Supporting materials). Such a course of the curve is connected with the inhibition of the enzymatic reaction, the beginning of which can be observed ca. 30 min after the enzyme injection. This phenomenon is probably connected with properties of the lysolipid generated by s-PLA2 from TMCL. In contrast to 2-lyso-DMPG and 2-lyso-DMPE 2,2′-dilyso-TMCL is completely water insoluble and remains at the air water interface, altering the organization of the Langmuir monolayer. The increasing presence of 2,2′-lyso-TMCL leads to the homogenization of the monolayer as indicated in the BAM experiments. Thus; the number of membrane defects is reduced affecting the docking of s-PLA2 to the model membrane. In 2016 we ordered 2,2′-dilyso-TMCL and some data for this phospholipids were published by us in the main paper [27] and in the associated Supporting materials. We decided to remind here these data regarding 2,2′-dilyso-TMCL in Langmuir monolayers and its mixtures with TMCL; thus all these data were added to the Supporting materials (the final part).

The temporal derivative of the mean molecular area $a = dA/dt$, that is the slope of the A-t curve in the burst phase can be treated as a measure of the rate of the enzymatic reaction [47]. In the case of the A-t curves for which the second region is strictly linear the straight line was fitted to the linear part of the curve and the *a* parameter was estimated with the application of linear regression. In the case of the sigmoidal curves, a steep and practically linear fragment can be observed at the beginning of the burst phase; thus, the straight line was first fit to this fragment. Additionally, a second straight line was fit to the less steep region of the sigmoid (ranging from $t = 40$ to $t = 60$ min). The lag times (t_L) and absolute values of the slope $|a|$ were gathered in Table 3. For the sigmoids the first *a* value was estimated from the fit to the steepest region of the curve, whereas the second value in brackets originates from the fit to the less steep region.

All the investigated model membranes here are formed by the mixing of two or three phospholipids: DMPG, DMPE and TMCL in the proportion described in the experimental of this article. The value of $|a|$ can be treated as a measure of the rate of the hydrolysis reaction catalyzed by s-PLA2; however, it should be done reasonably. For DMPG $|a|$ is 9 times (nearly one row of order) higher than for DMPE and 7 times than for TMCL. However, this does not mean explicitly that the rate of

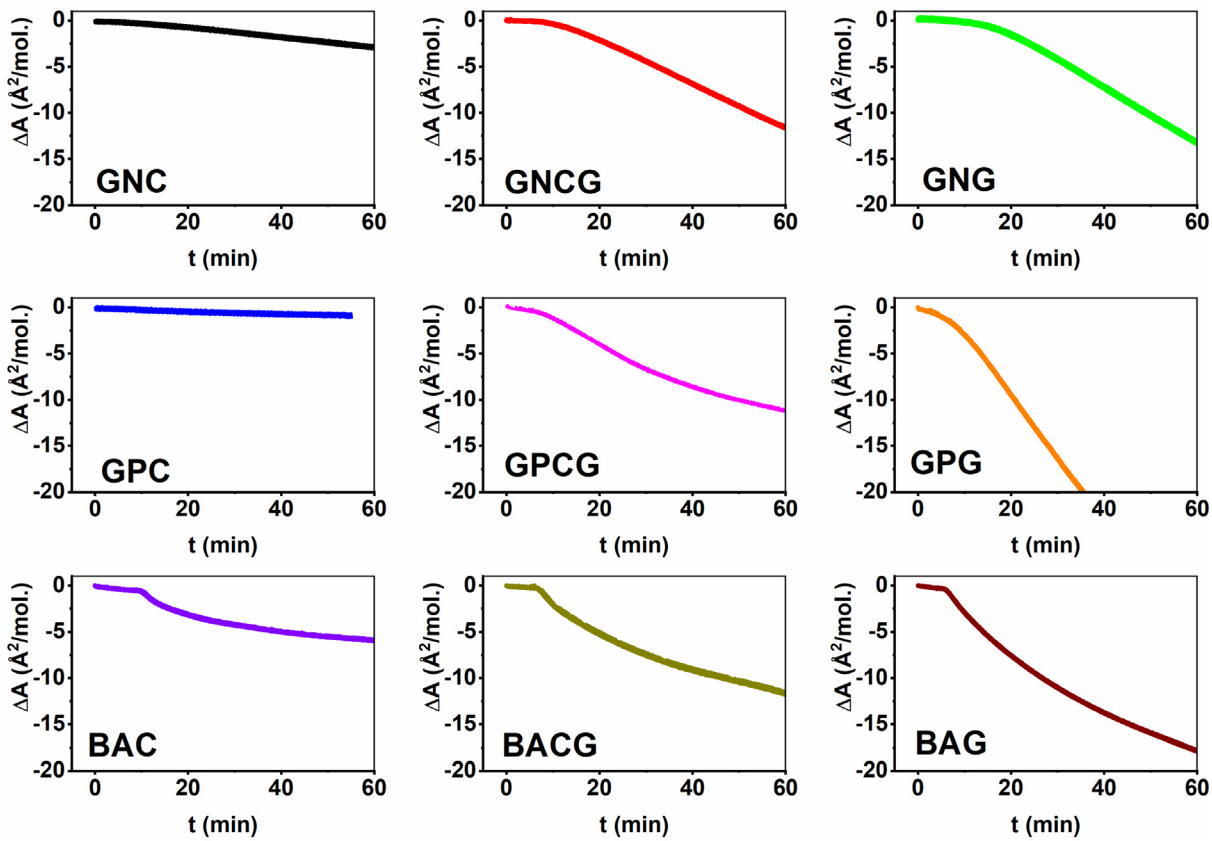

Fig. 6. A-t curves registered after the s-PLA2 solution injection below the model membranes. The experiments were repeated at least twice and the presented data are mean values of the performed experiments. The standard deviation of ΔA was not higher than 5%.

Table 3
Lag time (t_L) and $|a|$ parameter extracted from the course of the A-t curves and $|a_{calc}|$ calculated as a weighted average.

Model	t_L (min)	$\|a\|$	$\|a_{calc}\|$
GNC	15 (± 1)	0.05 (± 0.004)	0.18 (± 0.014)
GNCG	12 (± 0.5)	0.24 (± 0.01)	0.38 (± 0.022)
GNG	17 (± 2)	0.30 (± 0.02)	0.59 (± 0.026)
GPC	22 (± 3)	0.01 (± 0.002)	0.21 (± 0.012)
GPCG	9 (± 2)	0.28 (± 0.03), (0.11 (± 0.01))	0.74 (± 0.024), (0,69 (± 0.024))
GPG	9 (± 1)	0.69 (± 0.03)	1,28 (± 0.036)
BAC	10 (± 2)	0.34 (± 0.01), (0.07 (± 0.005))	0.55 (± 0.017), 0.45 (± 0.017)
BACG	6 (± 0.5)	0.38 (± 0.02), (0.17 (± 0.01))	0.89 (± 0.025), 0,82 (± 0.025)
BAG	7 (± 1)	0.64 (± 0.04), (0.31 (± 0.005))	1.29 (± 0.032), 1.27 (± 0.032)
DMPG	8.0 (± 1)	1.56 (± 0.04)	–
DMPE	25 (± 4)	0.17 (± 0.02)	–
TMCL	7 (± 1)	0.22 (± 0.01), (0.09 (± 0.01))	–

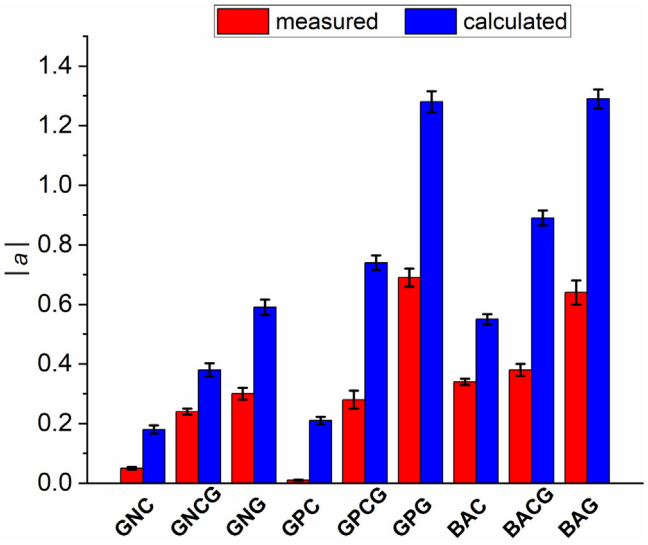

Fig. 7. Comparison of the measured $|a|$ and calculated $|a_{calc}|$ slopes of the A-t curves.

enzymatic hydrolysis of DMPG is 9 times greater than of DMPE. In our experiment we monitor the fall of mean molecular area in time keeping the constant pressure of 20 mN/m. The fall of A is mainly connected with the dissolution of the lysolipid in the tris-saline subphase. Lyso-DMPG has a large hydrophilic head-group of the glycerol molecule, so it is much better soluble in water than lyso-DMPE with a small ethanolamine headgroup. It turned out that the temporal evolution of the monolayer texture at 20 mN/m visualized by BAM for the DMPE monolayer (SFig12, Supporting materials) is very similar to the evolution of the DMPG monolayer [47]. However, in the first approximation if the specific interactions between the different phospholipid molecules were excluded it could be assumed that the $|a|$ for a binary or a ternary monolayer formed from DMPG, DMPE and TMCL should be a weighted average of the $|a|$ noticed for the one-component monolayers. Therefore; we calculated the theoretical value of $|a|$ as a weighted average following the composition of the model bacterial membranes. The values ($|a_{calc}|$) were gathered in the last column of Table 2, while in Fig. 7 the measured and calculate $|a|$ values were compared in the form of a column plot.

As it is visible in Fig. 7 the measured $|a|$ values are not weighted averages of the slopes of the A-t curves for the one-component monolayers. The measured slopes of the burst phase parts of the A-t curves are always smaller than the values calculated as the weighted average. For GNG, GPG, BACG and BAG the calculated values are approximately two times higher than the measured, while for GNCG and BAC the calculated value is higher approx. by one third than the measured. The largest differences between the calculated and measured $|a|$ values can be observed in the model membranes composed solely from DMPE and TMCL, that is GNC and GPC, from which the case of GPC is especially interesting as the enzyme could not practically degrade the phospholipid molecules forming this model membrane. The results are in accordance with the thermodynamic considerations of the 2D miscibility excess functions, as it was proved that in the system DMPE/TMCL the sign of ΔG^{exc} was negative suggesting attractive interactions between the phospholipid molecules, whereas in the system DMPG/TMCL the sign of ΔG^{exc} was positive denoting less beneficial interactions and possible separation of nanodomains enriched in a particular phospholipid. The energetically beneficial interactions between the zwitterionic DMPE molecule and the anionic phospholipid TMCL lead to more compact domains from which it is more difficult to s-PLA2 to withdraw the phospholipid molecules. Interestingly, GNC and GPC have a very similar mesoscopic texture, as visualized by BAM, and identical 2D crystalline structure, as proved by GIXD; thus, the differences in the s-PLA2 activity toward the model membranes is rather not connected with the membrane defects and the docking of the enzyme molecule, but with the transport of the phospholipid molecule into the active site the enzyme. Indeed, the too-high degree of order of the phospholipid molecules in the Langmuir monolayer can completely terminate the enzymatic reaction, as it was proved in the experiments performed on the phosphatidylcholine monolayers [65,66]. Moreover, these observations can also be connected with the differences in charge density in the head-group region in both systems. Cardiolipin has a relatively small headgroup with two negative charges located on it, so the density of the negative charge localized on the head-groups is much higher in the GPC than in the GNC model. In our studies two kinds of Gram-positive bacteria models were investigated: in the GP series the zwitterionic phospholipid DMPE was present at the fixed mole ratio of 20%, whereas the remaining 80% was reserved for the anionic phospholipids. In the case of the models from the BA series, the membranes were formed solely from anionic phospholipid molecules. In our tests of the activity of s-PLA2 it turned out that such membranes are less resistant to the attack of s-PLA2 than these containing the limited amount of DMPE.

To follow the degradative action of s-PLA2 toward the model bacterial membranes the evolution of their mesoscopic texture was monitored with the application of Brewster angle microscopy. The entire sequences of photos taken with the frequency of 10 min are presented in Supporting materials. Here we compare the image of the model membrane in $t = 0$, that is just after the enzyme injection and 60 min later. The selected BAM photos are presented in Fig. 8.

The selection of the BAM photos underlines the role of cardiolipin for the model membrane endurance to s-PLA2 activity. It can be realized that for the systems being the combination of TMCL and DMPE, that is GNC and GPC the photos taken 1 h after the injection of the enzyme are virtually identical as at $t = 0$. The only possible difference is the lower contribution of dark domains and crevices in the monolayer texture. The monolayers 60 min after PLA2 injection were more homogeneous and compact than at the beginning of the experiment which corroborates the earlier thesis that the liberation of lyso-TMCL lowers the number of membrane defects and by this lowers the activity of s-PLA2 with time elapse. The case of BAC, the model membrane formed entirely by anionic phospholipids is quite different. 60 min after the enzyme injection the area of the dark LE domains is greater than at the beginning of the experiment, meaning that lyso-TMCL partially separates from the condensed TMCL domains probably mixing with DMPG or lyso-DMPG molecules. By this new membrane defects are formed and the hydrolysis proceeds. However, as it was already discussed lyso-TMCL can also partially remain mixed with its mother compound, which finally leads to the sigmoidal shape of the A-t curve registered for the BAC model membrane. Regarding the ternary systems: GPCG and the equimolar binary system BACG a common conclusion can be drawn from the BAM images. 60 min after the enzyme injection the films are more homogeneous than at the beginning of the experiments. The observed phenomena indicate that the monolayers are more susceptible to s-PLA2 action than their counterparts not containing DMPG (GNC, GPC) or containing it on a lower level (BAC). The homogenization of the monolayer follows due to lyso-TMCL liberation and leads to the sigmoidal shape of the A-t curve registered for GPCG and BACG. The model membranes which completely do not contain cardiolipin, that is GNG and GPG are completely degraded 1 h after the beginning of the experiment. The characteristic texture of these membranes observed at $t = 0$ disappears and 60 min after the enzyme injection the images are dark with multiple large 3D aggregates formed probably by calcium myristate. Interestingly, the BAG model membrane behaves differently. DMPG dominates in this monolayer containing 75% of its molecules; however, the 25% of cardiolipin molecules seems to plays here a protective role. The $|a|$ value is initially high at the level of 0.642 but falls after 40 min to 0.315 to achieve 0.191 80 min after the enzyme injection. At the beginning of the experiment after the lag phase the slope of the A-t curve is high as lyso-DMPG dissolves quickly in the aqueous subphase. However, as cardiolipin is hydrolyzed much slower than DMPG and its hydrolysis product lyso-TMCL remains at the interface, the composition of the model membrane evolves with time. It is successively enriched in cardiolipin and lyso-cardiolipin. This leads to the proceeding homogenization of the monolayer leading to the sigmoidal shape of the A-t curve and the successive lowering of the hydrolysis rate with time.

4. Conclusions

Our studies performed on model bacterial membranes focused on the problem, how the mutual proportion of the three main phospholipid classes present in bacterial membranes affects their endurance to externally secreted membrane-lytic enzymes present in the soil. Snake venom s-PLA2 was applied as a model of highly active membrane degrading enzymes. The characterization of the mechanical properties of the 9 investigated models of soil bacteria membranes proved that the monolayers have similar elasticities, as the C_S^{-1}-π curves had qualitatively similar courses for all of the systems. The characterization of the mesoscopic properties of these monolayers performed with BAM proved that the evolution of the textures upon the monolayer compression was similar for all the 6 model membranes containing phosphatidylethanolamine, regardless its proportion. On the contrary significantly different textures of the condensed domains were observed for the model membranes of Gram-positive bacteria composed solely of the anionic phospholipids. The application of the GIXD technique proved that the condensed domains are 2D crystalline in all the 9 investigated model bacterial membranes and that the packing of the molecules within the monolayer plane is virtually the same regardless the membrane composition. Namely, for 7 of the 9 models the hexagonal lattice was determined and the length of the a period of the unit cell was very similar, giving practically the same area per hydrocarbon chain. Only for two models rich in DMPG (BAG and GPG) the tilt of the hydrocarbon chains from the monolayer normal was determined. Thus, a question arose if these model membranes so structurally similar had comparable resistivity to the attack of s-PLA2. It turned out, that the answer was no. Generally, the monolayers containing cardiolipin in higher proportion were much more resistant to the enzymatic degradation. The two model membranes devoid of cardiolipin: GNG and GPG were completely degraded by s-PLA2 1 h after the enzyme injection as proved by BAM. Interestingly in the BAG model in which DMPG consist the 75% of the

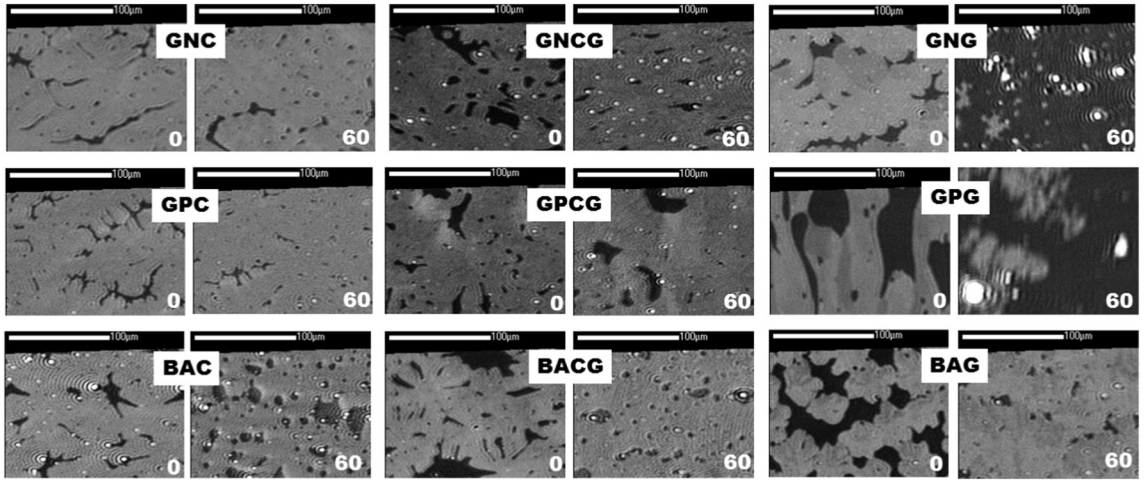

Fig. 8. Representative BAM images taken for the model bacterial membranes in the moment of s-PLA2 injection (0) and 60 min later.

phospholipid and TMCL only 25%, the degradation of the membrane was severely limited and retarded in time. Thus, it was clearly visible that the presence of cardiolipin protects the DMPG molecules against the enzymatic hydrolysis. Taking under consideration these results it could be hypothesized that the membrane composed solely of cardiolipins would be the most convenient protective barrier to Gram-positive bacteria. However, this thesis turned out to be false in the light of our experiments. The only model membrane which was not hydrolyzed by s-PLA2 in the applied experimental conditions was GPC, that is a binary monolayer composed in 80% of TMCL and in 20% of DMPE. The A-t curve and BAM images for one-component TMCL and DMPE monolayers proved that they were hydrolyzed by s-PLA2 and that their texture was modified by the presence of lysolipids. Mixed together as the GPC monolayer they were completely resistant to the hydrolytic activity of s-PLA2. The same cannot be said about the GNC model in which the proportion of TMCL to DMPE was reversed – for this model system the progress of the enzymatic reaction was clearly documented by the course of the A-t curve and the sequence of BAM images. For most of the model systems rich in cardiolipin the A-t curve had a sigmoidal course, proving the partial inhibition of the enzyme with time elapse. This observation was correlated with the progressing homogenization of these monolayers connected with the liberation of 2,2′-dilyso-TMCL. This lysolipid is water insoluble and its presence at the interface leads to the merge of the condensed domains leading to a monolayer poor in defects which are the natural docking sites for s-PLA2. Very interesting was also the comparison of the measured slopes $|a|$ of the A-t curves in the burst phase with the $|a|$ values calculated as a weighted averages of the slopes of the A-t curves registered for one-component phospholipid monolayers. It turned out that the mixed monolayers were always more resistant to s-PLA2 than the model membranes formed solely by one phospholipid class. This observation is in accordance with the experiments performed on the cell lines, mainly on *E. coli* with some genes knocked out [26,27]. *E. coli* completely devoid of one of the phospholipid classes could survive but was much more susceptible to pollutants, antibiotics and enzymes than the wild cell line. Summing up, our results underline the importance of cardiolipin both in the Gram-positive as well as in the Gram-negative bacteria membranes, but also prove that it is most effective in cooperation with phosphatidylethanolamines and that the presence of the limited amounts of the PE phospholipids in Gram-positive bacteria membranes is crucial for their durability.

Declaration of competing interest

I would like herby to certify on myself and on behalf of my co-authors that there are no conflicts of interests regarding our contribution entitled “The composition of phospholipid model bacterial membranes determines their endurance to secretory phospholipase A2 attack – the role of cardiolipin”. The studies referred in our article were financed by the Polish National Science Centre (No 2016/21/B/ST5/00245).

Acknowledgements

This project was financed by the National Science Centre (No 2016/21/B/ST5/00245). We gratefully acknowledge SOLEIL for provision of synchrotron radiation facilities and we would like to thank Dr. Philippe Fontaine for assistance in using SIRIUS beamline.

Appendix A. Supplementary data

π-A isotherms for the binary and ternary systems on the basis of which the thermodynamic considerations were performed. GIXD data for the remaining systems. A-t curves for the one-component phospholipid monolayers exposed to s-PLA2. Entire sets of the BAM images illustrating the temporal evolution of the texture of the model membranes after the injection of s-PLA2 to the subphase. Supplementary data to this article can be found online at doi:10.1016/j.bbamem.2020.183239.

References

[1] N. Fierer, R.B. Jackson, The diversity and biogeography of soil bacterial communities, PNAS 103 (2006) 626–631.
[2] L. Ranjard, S. Dequiedt, N. Chemidlin Prevost-Boure, J. Thioulouse, N.P.A. Saby, M. Lelievre, P.A. Maron, F.E.R. Morin, A. Bispo, C. Jolivet, D. Arrouays, P. Lemanceau, Turnover of soil bacterial diversity driven by wide-scale environmental heterogeneity, Nat. Commun. 4 (2013) 1434.
[3] E. Perez-Valera, M. Goberna, M. Verdu, Phylogenetic structure of soil bacterial communities predicts ecosystem functioning, FEMS Microbiol. Ecol. 91 (2015) 1–9.
[4] J.R. Jeon, K. Murugesan, P. Baldrian, S. Schmidt, Y.S. Chang, Aerobic bacterial catabolism of persistent organic pollutants — potential impact of biotic and abiotic interaction, Curr. Opin. Biotechnol. 38 (2016) 71–78.
[5] W.R. Abraham, B. Nogales, P.N. Golyshin, D.H Pieper, K.N. Timmis, Polychlorinated biphenyl-degrading microbial communities in soils and sediments, Curr. Opin. Microbiol. 5 (2002) 246–253.
[6] J.A. Field, R. Sierra-Alvarez, Microbial degradation of chlorinated dioxins, Chemosphere 71 (2008) 1005–1018.
[7] R.A. Kanaly, S. Harayama, Advances in the field of high-molecular-weight polycyclic aromatic hydrocarbon biodegradation by bacteria, Microb. Biotechnol. 3 (2010) 136–164.
[8] S. Kim, F. Picardal, Microbial growth on dichlorobiphenyls chlorinated on both rings as a sole carbon and energy source, Appl. Environ. Microbiol. 67 (2001) 1953–1955.
[9] F.P. Chavez, H. Lunsdorf, C.A. Jerez, Growth of polychlorinated-biphenyl-degrading bacteria in the presence of biphenyl and chlorobiphenyls generates oxidative stress and massive accumulation of inorganic polyphosphate, Appl. Environ. Microbiol. 70 (2004) 3064–3072.
[10] S.A. Jang, D.S. Lee, M.W. Lee, S.H. Woo, Toxicity of phenanthrene dissolved in

nonionic surfactant solutions to Pseudomonas putida P2, FEMS Microbiol. Lett. 267 (2007) 194–199.
[11] P. Martínez, L. Agullo, M. Hernandez, M. Seeger, Chlorobenzoate inhibits growth and induces stress proteins in the PCB-degrading bacterium *Burkholderia xenovorans* LB400, Arch. Microbiol. 188 (2007) 289–297.
[12] M. Sánchez, F.J. Aranda, J.A. Teruel, M.J. Espuny, A. Marqués, A. Manresa, A. Ortiz, Permeabilization of biological and artificial membranes by a bacterial dirhamnolipid produced by *Pseudomonas aeruginosa*, J. Colloid Interface Sci. 341 (2010) 240–247.
[13] J.L. Li, B.H. Chen, Surfactant-mediated biodegradation of polycyclic aromatic hydrocarbons, Materials 2 (2009) 76–94.
[14] S. Zoradova, H. Dudasova, Lucia Lukacova, K. Dercova, M. Certík, The effect of polychlorinated biphenyls (PCBs) on the membrane lipids of *Pseudomonas stutzeri*, Int. Biodeter. Biodeg. 65 (2011) 1019–1023.
[15] M. Broniatowski, M. Binczycka, A. Wójcik, M. Flasiński, P. Wydro, Polycyclic aromatic hydrocarbons in model bacterial membranes – Langmuir monolayer studies, Biochim. Biophys. Acta Biomembr. 1858 (2016) 2402–2412.
[16] R.H. Schaloske, E.A. Dennis, The phospholipase A2 superfamily and its group numbering system, Biochim. Biophys. Acta 1761 (2006) 1246–1259.
[17] M. Sugiyama, K. Ohtani, M. Izuhara, T. Koike, K. Suzuki, S. Imamura, H. Misaki, A novel prokaryotic phospholipase A2, J. Biol. Chem. 277 (2002) 20051–20058.
[18] P.J. Sutherland, A.E. Tobin, C.L. Rutherford, N.P.J. Price, *Dictyostelium discoideum* fatty-acyl amidase II has deacylase activity on *Rhizobium* nodulation factors, J. Biol. Chem. 273 (1998) 4459–4464.
[19] U. Jankiewicz, U. Szawłowska, M. Sobańska, Biochemical characterization of an alkaline metallopeptidase secreted by a *Pseudomonas fluorescens* isolated from soil, J. Basic Microbiol. 50 (2010) 125–134.
[20] R.I. Evans, P.J. McClure, G.W. Gould, N.J. Russell, The effect of growth temperature on the phospholipid and fatty acyl compositions of non-proteolytic *Clostridium botulinum*, Int. J. Food Microbiol. 40 (1998) 159–167.
[21] L.Y. Baker, C.R. Hobby, A.W. Siv, W.C. Bible, M.S. Glennon, D.M. Anderson, S.J. Symes, D.K. Giles, Pseudomonas aeruginosa responds to exogenous polyunsaturated fatty acids (UFAs) by modifying phospholipid composition, membrane permeability, and phenotypes associated with virulence, BMC Microbiol. 18 (2018) 117.
[22] C.S. Lopez, A.F. Alice, H. Heras, E.A. Rivas, C. Sanchez-Rivas, Role of anionic phospholipids in the adaptation of Bacillus subtilis to high salinity, Microbiol. 152 (2006) 605–616.
[23] A. Kallimanis, S. Frillingos, C. Drainas, A.I. Koukkou, Taxonomic identification, phenanthrene uptake activity, and membrane lipid alterations of the PAH degrading Arthrobacter sp. strain Sphe3, Appl Microbiol Biotechnol. 76 (2007) 709–717.
[24] R.F. Epand, P.B. Savage, R.M. Epand, Bacterial lipid composition and the antimicrobial efficacy of cationic steroid compounds (Ceragenins), Biochim. Biophys. Acta 1768 (2007) 2500–2509.
[25] T.H.P. Nguyen, Y.T.H. Pham, S.H. Nguyen, V. Baulin, R.J. Croft, B. Phillips, R.J. Crawford, E.P. Ivanova, The bioeffects resulting from prokaryotic cells and yeast being exposed to an 18 GHz electromagnetic field, PLoS One 11 (2016) e0158135.
[26] W. Dowhan, A retrospective: use of Escherichia coli as a vehicle to study phospholipid synthesis and function, Biochim. Biophys. Acta 1831 (2013) 471–494.
[27] K. Matsumoto, Dispensable nature of phosphatidylglycerol in Escherichia coli: dual roles of anionic phospholipids, Molec. Microbiol. 39 (2001) 1427–1433.
[28] M.C. Trombe, M.A. Laneelle, G. Laneelle, Lipid composition of aminopterin-resistant and sensitive strains of *Streptococcus pneumoniae*. Effect of aminopterin inhibition, Biochim. Biophys. Acta 574 (1979) 290–300.
[29] M. Cohen, C. Panos, Membrane lipid composition of Streptococcus pyogenes and derived L form, Biochemistry 5 (1966) 2385–2392.
[30] L. Hernández-Villa, M. Manrique-Moreno, C. Leidy, M. Jemioła-Rzemińska, C. Ortíze, K. Strzałka, Biophysical evaluation of cardiolipin content as a regulator of the membrane lytic effect of antimicrobial peptides, Biophys. Chem. 238 (2018) 8–15.
[31] Z.D. Dalebroux, M.B. Edrozo, R.A. Pfuetzner, S. Ressl, B.R. Kulasekara, M.P. Blanc, S.I. Miller, Delivery of cardiolipins to the *Salmonella* outer membrane is necessary for survival within host tissues and virulence, Cell Host Microbe 17 (2015) 441–451.
[32] T. Romantsov, Z. Guan, J.M. Wood, Cardiolipin and the osmotic stress responses of bacteria, Biochim. Biophys. Acta 1788 (2009) 2092–2100.
[33] G. Sautrey, M. El Khoury, A. Giro dos Santos, L. Zimmermann, M. Deleu, L. Lins, J.L. Decout, M.P. Mingeot-Leclercq, Negatively charged lipids as a potential target for new amphiphilic aminoglycoside antibiotics, J. Biol. Chem. 291 (2016) 13864–13874.
[34] S. Lopes, C.S. Neves, P. Eaton, P. Gameiro, Cardiolipin, a key component to mimic the *E. coli* bacterial membrane in model systems revealed by dynamic light scattering and steady-state fluorescence anisotropy, Anal. Bioanal. Chem. 398 (2010) 1357–1366.
[35] J. Hoyo, J. Torrent-Burgués, T. Tzanov, Physical states and thermodynamic properties of model gram-negative bacterial inner membranes, Chem. Phys. Lipids 218 (2019) 57–64.
[36] P. Wydro, The influence of cardiolipin on phosphatidylglycerol/phosphatidylethanolamine monolayers—studies on ternary films imitating bacterial membranes, Colloids Surf. B: Biointerfaces 106 (2013) 217–223.
[37] A. Clausell, M. Garcia-Subirats, M. Pujol, M.A. Busquets, F. Rabanal, Y. Cajal, Gram-negative outer and inner membrane models: insertion of cyclic cationic lipopeptide, J. Phys. Chem. B 111 (2007) 551–563.
[38] M. Derde, F. Nau, C. Guérin-Dubiard, V. Lechevalier, G. Paboeuf, S. Jan, F. Baron, M. Gautier, V. Vié, Native and dry-heated lysozyme interactions with membrane lipid monolayers: lipid packing modifications of a phospholipid mixture, model of the Escherichia coli cytoplasmic membrane, Biochim. Biophys. Acta 1848 (2015) 1065–1073.
[39] D. Gidalevitz, Y. Ishitsuka, A.S. Muresan, O. Konovalov, A.J. Waring, R.I. Lehrer, K.Y.C. Lee, Interaction of antimicrobial peptide protegrin with biomembranes, PNAS 100 (2003) 6302–6307.
[40] G.A. Lopez, R.M. Heredia, P.S. Boeris, G.I. Lucchesi, Content of cardiolipin of the membrane and sensitivity to cationic surfactants in Pseudomonas putida, J. Appl. Microbiol. 121 (2016) 1004–1014.
[41] D. Vollhardt, Brewster angle microscopy: a preferential method for mesoscopic characterization of monolayers at the air/water interface, Curr. Opin. Colloid Interface Sci. 19 (2014) 183–197.
[42] W. Daear, M. Mahadeo, E.J. Prenner, Applications of Brewster angle microscopy from biological materials to biological systems, Biochim. Biophys. Acta 1859 (2017) 1749–1766.
[43] K.M. Maloney, M. Grandbois, D.W. Grainger, C. Salesse, K.A. Lewis, M.F. Roberts, Phospholipase A2 domain formation in hydrolyzed asymmetric phospholipid monolayers at the air/water interface, Biochim. Biophys. Acta 1235 (1995) 395–405.
[44] U. Dahmen-Levison, G. Brezesinski, H. Mohwald, Specific adsorption of PLA2 at monolayers, Thin Solid Films 327–329 (1998) 616–620.
[45] M. Gudmand, S. Rocha, N.S. Hatzakis, K. Peneva, K. Mullen, D. Stamou, H. Uji-I, J. Hofkens, T. Bjornholm, T. Heimburg, Influence of lipid heterogeneity and phase behavior on phospholipase A2 action at the single molecule level, Biophys. J. 98 (2010) 1873–1882.
[46] E. Berring, S. Brancato, K. Grant, E. Schaper, S. Kadavil, H. Smagin, S.O. Hatic II, W. Picking, A. Barnoski Serfis, Destabilization of phospholipid model membranes by YplA, a phospholipase A2 secreted by *Yersinia enterocolitica*, Chem. Phys. Lipids 131 (2004) 135–149.
[47] M. Broniatowski, M. Urbaś, Interactions of two structurally related anionic phospholipids cardiolipin and phosphatidylglycerol with phospholipase A2. Langmuir monolayer studies, Biochim. Biophys. Acta Biomem. 1859 (2017) 155–156.
[48] J.T. Davies, E.K. Rideal, Interfacial Phenomena, New York, Academic Press, 1961.
[49] I.S. Costin, G.T. Barnes, Two-component monolayers. II. Surface pressure—area relations for the octadecanol—docosyl sulphate system, J. Colloid Interface Sci. 51 (1975) 106–121.
[50] F. Prossnigg, A. Hickel, G. Pabst, K. Lohner, Packing behaviour of two predominant anionic phospholipids of bacterial cytoplasmic membranes, Biophys. Chem. 150 (2010) 129–135.
[51] A. Wójcik, M. Pawłowski, P. Wydro, M. Broniatowski, Effects of polychlorinated pesticides and their metabolites on phospholipid organization in model microbial membranes, J. Phys. Chem. B 122 (2018) 12017–12030.
[52] F. Etienne, Y. Roche, P. Peretti, S. Bernard, Cardiolipin packing ability studied by grazing incidence X-ray diffraction, Chem. Phys. Lipids 152 (2008) 13–23.
[53] M. Broniatowski, K. Sobolewska, M. Flasiński, P. Wydro, Studies on the interactions of bisphenols with anionic phospholipids of decomposer membranes in model systems, Biochim. Biophys. Acta 1858 (2016) 756–766.
[54] C.A. Helm, P. Tippmann-Krayer, H. Möhwald, J. Als-Nielsen, K. Kjaer, Phases of phosphatidyl ethanolamine monolayers studied by synchrotron x-ray scattering, Biophys. J. 60 (1991) 1457–1476.
[55] J. Als-Nielsen, D. Jacquemain, K. Kjaer, F. Leveiller, M. Lahav, L. Leiserowitz, Principles and applications of grazing incidence X-ray and neutron scattering from ordered molecular monolayers at the air-water interface, Phys. Rep. 246 (1994) 251–313.
[56] Y. Matoba, Y. Katsube, M. Sugiyama, The crystal structure of prokaryotic phospholipase A2, J. Biol. Chem. 277 (2002) 20059–20069.
[57] Y. Matoba, M. Sugiyama, Atomic resolution structure of prokaryotic phospholipase A2: analysis of internal motion and implication for a catalytic mechanism, Proteins 51 (2003) 453–469.
[58] G. Brezesinski, H. Mohwald, Langmuir monolayers to study interactions at model membrane surfaces, Adv. Colloid Interf. Sci. 100–102 (2003) 563–584.
[59] L.K. Nielsen, J. Risbo, T.H. Callisen, T. Bjornholm, Lag-burst kinetics in phospholipase A2 hydrolysis of DPPC bilayers visualized by atomic force microscopy, Biochim. Biophys. Acta 1420 (1999) 266–271.
[60] S. Gallier, E. Shaw, J. Cuthbert, D. Gragson, H. Singh, R. Jiménez-Flores, Hydrolysis of milk phospholipid and phospholipid–protein monolayers by pancreatic phospholipase A2, Food Res. Int. 54 (2013) 718–725.
[61] L. De Tullio, M.L. Fanani, B. Maggio, Surface mixing of products and substrate of PLA2 in enzyme-free mixed monolayers reproduces enzyme-driven structural topography, Biochim. Biophys. Acta 1828 (2013) 2056–2063.
[62] Y. Corvis, B. Korchowiec, G. Brezesinski, S. Follot, E. Rogalska, Impact of aluminum on the oxidation of lipids and enzymatic lipolysis in monomolecular films at the air/water interface, Langmuir 23 (2007) 3338–3348.
[63] M. Grandbois, H. Clausen-Schaumann, H. Gaub, Atomic force microscope imaging of phospholipid bilayer degradation by phospholipase A2, Biophys. J. 74 (1998) 2398–2404.
[64] U. Dahmen-Levison, G. Brezesinski, Methyl-branched glycerophosphocholines: monolayer disorder and its effect on the rate of phospholipase A2 catalyzed hydrolysis, Phys. Chem. Chem. Phys. 2 (2000) 4605–4608.
[65] K. Czapla, B. Korchowiec, M. Orlof, J. Rubio Magnieto, E. Rogalska, Enzymatic probing of model lipid membranes: phospholipase A2 activity toward monolayers modified by oxicam NSAIDs, J. Phys. Chem. B 115 (2011) 9290–9298.
[66] C.S. Rao, S. Damodaran, Surface pressure dependence of phospholipase A2 activity in lipid monolayers is linked to interfacial water activity, Colloids Surfaces B Biointerfaces 34 (2004) 197–204.